Stefanini, S., Desideri, A., Vecchini, P., Drakenberg, T., & Chiancone, E. (1989) *Biochemistry 28*, 378–382.
Theil, E. C. (1987) *Annu. Rev. Biochem. 56*, 289–315.
Theil, E. C. (1989) *Adv. Enzymol. Relat. Areas Mol. Biol. 63*, 421–449.
Tipton, P. A., McCracken, J., Cornelius, J. B., & Peisach, J. (1989) *Biochemistry 28*, 5720–5728.
Treffry, A., & Harrison, P. M. (1984) *J. Inorg. Biochem. 21*, 9–20.
Treffry, A., Harrison, A., Luzzago, A., & Cesareni, G. (1989) *FEBS Lett. 247*, 268–272.
van Willigen, H. (1980) *J. Magn. Reson. 39*, 37–46.
Wardeska, J. G., Viglione, B., & Chasteen, N. D. (1986) *J. Biol. Chem. 261*, 6677–6683.
Watt, G. D., Frankel, R. B., & Papaefthymoiu, G. C. (1985) *Proc. Natl. Acad. Sci. U.S.A. 82*, 3640–3643.
Yang, C. Y., Meagher, A., Huynh, B. H., Sayers, D. E., & Theil, E. C. (1989) *Biochemistry 26*, 497–503.

Secondary Structure and Side-Chain ^1H and ^{13}C Resonance Assignments of Calmodulin in Solution by Heteronuclear Multidimensional NMR Spectroscopy†

Mitsuhiko Ikura,‡ Silvia Spera,‡,§ Gaetano Barbato,‡,∥ Lewis E. Kay,‡ Marie Krinks,⊥ and Ad Bax*,‡

Laboratory of Chemical Physics, National Institute of Diabetes and Digestive and Kidney Diseases, and Laboratory of Biochemistry, National Cancer Institute, National Institutes of Health, Bethesda, Maryland 20892

Received April 9, 1991; Revised Manuscript Received June 28, 1991

ABSTRACT: Heteronuclear 2D and 3D NMR experiments were carried out on recombinant *Drosophila* calmodulin (CaM), a protein of 148 residues and with molecular mass of 16.7 kDa, that is uniformly labeled with ^{15}N and ^{13}C to a level of >95%. Nearly complete ^1H and ^{13}C side-chain assignments for all amino acid residues are obtained by using the 3D HCCH-COSY and HCCH-TOCSY experiments that rely on large heteronuclear one-bond scalar couplings to transfer magnetization and establish through-bond connectivities. The secondary structure of this protein in solution has been elucidated by a qualitative interpretation of nuclear Overhauser effects, hydrogen exchange data, and $^3J_{HNH\alpha}$ coupling constants. A clear correlation between the $^{13}C\alpha$ chemical shift and secondary structure is found. The secondary structure in the two globular domains of *Drosophila* CaM in solution is essentially identical with that of the X-ray crystal structure of mammalian CaM [Babu, Y., Bugg, C. E., & Cook, W. J. (1988) *J. Mol. Biol. 204*, 191–204], which consists of two pairs of a "helix–loop–helix" motif in each globular domain. The existence of a short antiparallel β-sheet between the two loops in each domain has been confirmed. The eight α-helix segments identified from the NMR data are located at Glu-6 to Phe-19, Thr-29 to Ser-38, Glu-45 to Glu-54, Phe-65 to Lys-77, Glu-82 to Asp-93, Ala-102 to Asn-111, Asp-118 to Glu-127, and Tyr-138 to Thr-146. Although the crystal structure has a long "central helix" from Phe-65 to Phe-92 that connects the two globular domains, NMR data indicate that residues Asp-78 to Ser-81 of this central helix adopt a nonhelical conformation with considerable flexibility.

Recent progress in NMR methodology has made it possible to obtain complete ^1H, ^{13}C, and ^{15}N resonance assignments for proteins in the 15–25-kDa molecular mass range, which constitutes a prerequisite for determining the 3D solution structure. Isotope-editing techniques combined with 2D NMR have been used successfully for recombinant proteins such as staphylococcal nuclease (18 kDa) (Torchia et al., 1989; Wang et al., 1990), *Escherichia coli* Trp repressor (a symmetric dimer of 25 kDa with 107 residues) (Arrowsmith et al., 1990), and T4 lysozyme (18.7 kDa) (McIntosh et al., 1990). This type of approach requires preparation of a large number of protein samples with selective isotope labeling of different amino acid types in the various protein preparations, a labor intensive and time-consuming process. More recent approaches, on the other hand, utilize uniform labeling with ^{15}N or ^{13}C in combination with 2D and 3D techniques. The 3D NOESY-HMQC experiment is an important example of this

Table I: Location of α-Helices in Calmodulin-$4Ca^{2+}$ Determined by NMR and X-ray Diffraction

α-helix	residue range	
	NMR[a]	X-ray[b]
I	E6–F19	T5–F19
II	T29–S38	T29–S38
III	E45–E54	E45–V55
IV	F65–K77	F65–F92
V	E82–D93	
VI	A102–N111	A102–N111
VII	D118–E127	D118–A128
VIII	Y138–T146	Y138–S147

[a] Present work. The experimental conditions are 0.1 M KCl, pH 6.3, at 36 °C. [b] Babu et al. (1988). The crystals were obtained from 45–60% (v/v) 2-methyl-2,4-pentanediol containing 50 mM cacodylate buffer, pH 5.6.

† This work was supported by the Intramural AIDS-Directed Antiviral Program of the Office of the Director of the National Institutes of Health. L.E.K. acknowledges a Centennial Fellowship from the Medical Research Council of Canada and the Alberta Heritage Trust Foundation. G.B. acknowledges a fellowship from Facolta di Scienze, Napoli Dottorato di Ricerca in Scienze Chimiche.

* To whom correspondence should be addressed.
‡ NIDDK, NIH.
§ Present address: Istituto Guido Donegani, Via Fauser 4, Novara, Italy.
∥ On leave from Universita di Napoli, Federico II, Dipartimento di Chimica, Via Mezzocannone 4, Naples, Italy.
⊥ National Cancer Institute, NIH.

0006-2960/91/0430-9216$02.50/0

approach and is applied to uniformly ^{15}N-labeled proteins (Marion et al., 1989; Zuiderweg & Fesik, 1989; Messerle et al., 1989). Clear demonstrations of this approach have been reported for interleukin-1β (17 kDa) (Driscoll et al., 1990), for staphylococcal nuclease (Torchia et al., 1989), and for calmodulin (CaM)[1] (Ikura et al., 1990d). Although recording a 3D ^{15}N-edited NOESY-HMQC spectrum is relatively simple, it frequently does not entirely solve the resonance assignment problem. Either the absence of observable sequential NOE connectivities or substantial degeneracy in the CαH region of the ^1H spectrum constitute major problems with this approach. More recently a different approach has been reported, which uses ^1H, ^{13}C, ^{15}N triple-resonance 3D NMR techniques for proteins that are uniformly enriched with both ^{15}N and ^{13}C (Ikura et al., 1990b, 1991; Kay et al., 1990b). This approach is quite straightforward for obtaining backbone ^1H, ^{13}C, and ^{15}N assignments, because it is not based on through-space NOE interactions but relies on large and uniform one-bond J couplings. Successful applications of the new approach have been demonstrated for CaM (Ikura et al., 1990b) and for its complex with a 26-residue myosin light-chain kinase fragment (Ikura et al., 1991).

CaM is a ubiquitous Ca^{2+}-binding protein that transmits information of the second messenger Ca^{2+} into a variety of calcium-dependent intracellular processes. It consists of 148 amino acids and has a molecular mass of 16.7 kDa. The X-ray crystal structure of CaM has been reported previously (Babu et al. 1988; Kretsinger et al., 1986) and shows an unusual "dumbbell" shape. The two globular lobes of the dumbbell, each of which is composed of a pair of the helix–loop–helix "EF-hand" Ca^{2+}-binding motif (Moews & Kretsinger, 1975), are connected by a long central helix. Small-angle X-ray scattering studies of CaM in solution (Seaton et al., 1985; Heidorn & Trewhella, 1988; Matsushima et al., 1989) showed that the two lobes are significantly (5–10 Å) closer together than in the crystal structure, suggesting bending of the central helix or a high degree of flexibility in this helix. In order to elucidate more details of the static and dynamic structure of calmodulin in solution, we have initiated the NMR study of this protein (Ikura et al., 1990b,d).

Here we report complete ^1H and ^{13}C side-chain assignments and present the secondary structure of CaM in solution. The side-chain ^1H and ^{13}C resonance assignments were obtained by means of a combination of the 3D ^1H–^{13}C–^{13}C–^1H (HCCH) COSY (Kay et al., 1990a; Bax et al., 1990a) and HCCH-TOCSY (Bax et al., 1990b) experiments. The secondary structure of this protein in solution is characterized on the basis of NOE data and $^3J_{HN\alpha}$ coupling constants. The ^{13}C chemical shift data confirm a recent report by Spera and Bax (1991) which indicates that $^{13}C\alpha$ and $^{13}C\beta$ chemical shifts are clear markers for secondary structure. In analogy with the X-ray crystal structure, CaM in solution is composed of four repeats of a helix–loop–helix segment. The first and second loop are connected by a short antiparallel β-sheet, and so are the third and fourth loop. The present NMR data suggest, however, that in solution the "central helix" found in the crystal structure has a significant deviation from α-helical geometry in the region Asp-78 to Ser-81.

Experimental Procedures

Sample Preparation. Recombinant *Drosophila* CaM was prepared with *E. coli* (strain AR58) harboring the pAS expression vector (Shatzman & Rosenberg, 1985). Uniform ^{15}N and ^{13}C labeling to a level of >95% was obtained by growing the bacteria in M9 minimal medium with [^{15}N]NH_4Cl (Isotec Inc.) and [$^{13}C_6$]D-glucose (MSD Isotopes) as the sole nitrogen and carbon sources, respectively. The protein was purified as described previously (Ikura et al., 1990b). For the NMR experiments, two samples were used: one contained 1.0 mM uniformly ^{15}N- and ^{13}C-labeled CaM in 99.9% D_2O, 4.1 mM $CaCl_2$, and 100 mM KCl, pH 6.3; the other contained 1.5 mM uniformly ^{15}N-labeled CaM in 95% H_2O/5% D_2O, 6.1 mM $CaCl_2$, and 100 mM KCl, pH 6.3.

NMR Spectroscopy. All NMR experiments were carried out at 36 °C on Bruker AM-600 or AM-500 spectrometers operating in the "reverse" mode. All 3D NMR data were processed on Sun-4 or Sun Sparc-1 workstations using a simple in-house written routine for F_2 Fourier transformation together with the commercially available software package NMR2 (New Methods Research, Inc., Syracuse, NY) for processing the F_1–F_3 planes, as described previously (Kay et al., 1989).

The pulse sequences used for the 3D HCCH-COSY (Kay et al., 1990a; Bax et al., 1990a) and HCCH-TOCSY (Bax et al., 1990b) experiments have been described in detail previously. A total of 64 complex t_1 (^1H), 32 complex t_2 (^{13}C), and 512 real t_3 (^1H) data points were collected for both experiments with acquisition times of 25.6 (t_1), 10.7 (t_2), and 51.2 ms (t_3). The ^1H and ^{13}C carriers were positioned at 2.61 and 43 ppm, respectively. The total measurement time for each experiment was approximately 36 h. Zero-filling was employed to yield a final absorptive spectrum of 256 × 64 × 512 data points. The weighting function applied in the F_1 and F_3 dimensions was a 60°-shifted sine bell function, while a 45°-shifted sine bell function was used in the F_2 dimension.

The pulse sequences used for the ^{15}N-separated 3D NOESY-HMQC (Fesik & Zuiderweg, 1988; Marion et al., 1989) and 3D ROESY-HMQC (Clore et al., 1990b) experiments have been reported previously. The NOESY-HMQC spectra were recorded at 500 MHz with 50-ms and 100-ms NOE mixing times, while the ROESY-HMQC spectrum was recorded at 600 MHz with a 33-ms ROE mixing time. CaM labeled only with ^{15}N was used for this set of experiments. A total of 128 complex t_1 (^1H), 32 complex t_2 (^{15}N), and 1024 real t_3 (^1H) data points were collected for both NOESY-HMQC and ROESY-HMQC experiments with acquisition times of 21.4 (t_1), 13.4 (t_2), and 51.2 ms (t_3). The ^1H carrier was positioned at 4.67 ppm and the ^{15}N carrier at 120 ppm. The total measurement time for each experiment was approximately 70 h. Zero-filling was employed to yield a final absorptive spectrum of 512 × 64 × 512 data points. In each dimension, a 60°-shifted sine bell weighting function was used.

The pulse sequence used for the 3D [^{15}N,^{15}N,^1H]HMQC-NOESY-HMQC experiment has been described in detail previously (Ikura et al., 1990a). The NOE mixing time was set to 140 ms. The ^1H and ^{15}N carriers were positioned at

[1] Abbreviations: CaM, calmodulin; COSY, correlated spectroscopy; HOHAHA, homonuclear Hartmann–Hahn spectroscopy; TOCSY, total correlated spectroscopy; HMQC, heteronuclear multiple-quantum correlation spectroscopy; HNCO, 3D HN–^{15}N–C′ correlation spectroscopy; HCACO, 3D CαH–$^{13}C\alpha$–C′ correlation spectroscopy; HCCH-COSY, 3D ^1H–^{13}C–^{13}C–^1H correlation spectroscopy via $^1J_{CC}$ carbon couplings; HCCH-TOCSY, 3D ^1H–^{13}C–^{13}C–^1H total correlation spectroscopy with isotropic mixing of ^{13}C magnetization; ^{13}C NOESY-HMQC, 3D ^1H–^1H nuclear Overhauser effect ^{13}C–^1H multiple-quantum coherence spectroscopy; ^{15}N NOESY-HMQC, 3D ^1H–^1H nuclear Overhauser effect ^{15}N–^1H multiple-quantum coherence spectroscopy; ^{15}N ROESY-HMQC, 3D ^1H–^1H rotating-frame nuclear Overhauser effect ^{15}N–^1H multiple-quantum coherence spectroscopy; ^{15}N HOHAHA-HMQC, 3D ^1H–^1H homonuclear Hartmann–Hahn ^{15}N–^1H multiple-quantum coherence spectroscopy; [^{15}N,^{15}N,^1H]HMQC-NOESY-HMQC, 3D ^{15}N–^1H multiple-quantum coherence ^1H–^1H nuclear Overhauser effect ^1H–^{15}N multiple-quantum coherence spectroscopy; NOE, nuclear Overhauser effect; TPPI, time-proportional phase increment.

4.67 and 116.5 ppm, respectively. The acquired 3D data matrix comprised 64 complex (t_1) × 32 complex (t_2) × 1024 real (t_3) data points, and the total measuring time was ~91 h. The spectral width was 1666 Hz in F_1 and F_2 and 8064 Hz in the F_3 dimension, with corresponding acquisition times of 38.4, 19.2, and 63.5 ms. The t_2 data were extended to 64 complex points by using linear prediction, and in addition, zero-filling was employed in all dimensions. The absorptive part of the final processed data matrix comprised 256 × 128 × 1024 points.

The ^1H–^{15}N HMQC-J experiment (method B) was carried out for measuring $^3J_{HN\alpha}$ coupling constants (Kay & Bax, 1990a). A total of 800 real t_1 (^{15}N) and 1024 real t_2 (^1H) data points were collected with acquisition times of 160 and 128 ms, respectively. Zero-filling was employed to yield an absorptive 2D matrix of 2048 × 2048 data points. The values of the $^3J_{NH\alpha}$ coupling constants were obtained from the splitting of the cross peaks in the F_1 dimension by using a correction procedure described previously (Kay & Bax, 1990a).

The ^1H–^{15}N HMQC experiment was used to identify slowly exchanging amide protons (Marion et al., 1989). A total of 128 complex t_1 (^{15}N) and 512 real t_2 (^1H) data points were collected with acquisition times of 64.0 and 63.5 ms, respectively. Zero-filling was employed to yield an absorptive 2D matrix of 256 × 512 data points. Data acquisitions for the HMQC spectra were started 5, 15, 35, 88, 228, 348, 608, and 1354 min after the protein was dissolved in D_2O. The measuring time for each of the 2D spectra was 10, 20, 40, 80, 80, 80, 80, and 80 min, respectively. The hydrogen exchange experiments were carried out at pH 6.75 and 25 °C.

The ^1H–^{13}C HMQC experiment was performed with the pulse sequence of Bendall et al. (1983) and Bax et al. (1983). A total of 256 complex t_1 (^{13}C) and 512 real t_2 (^1H) data points were collected with acquisition times of 15.4 and 63.5 ms, respectively. Zero-filling was employed to yield an absorptive 2D matrix of 512 × 512 data points.

Results and Discussion

Side-Chain ^1H and ^{13}C Assignments. The polypeptide backbone HN, ^{15}N, $^{13}C\alpha$, CαH, and $^{13}C'$ chemical shifts of Ca^{2+}-ligated CaM in 0.1 M KCl, pH 6.3, at 47 °C, obtained from triple-resonance 3D NMR experiments, were previously reported (Ikura et al., 1990b). The present study extends the backbone spin systems to the side chains, using the HCC-H-COSY (Kay et al., 1990a; Bax et al., 1990a) and HCC-H-TOCSY (Bax et al., 1990b) techniques. It should be noted, however, that the triple-resonance backbone assignment procedure also requires unambiguous amino acid type assignments for a limited number of residues. In our recent study of CaM complexed with a 26-residue myosin light-chain kinase fragment, these amino acid type assignments were derived from HCCH experiments (Ikura et al., 1991). Therefore, the triple-resonance techniques and the HCCH methods are used in an integrated manner to obtain the complete assignment of both backbone and side-chain resonances in proteins.

In the HCCH experiments, magnetization transfer is achieved in three steps; (i) ^1H magnetization is transferred to its directly bonded ^{13}C nucleus via $^1J_{CH}$ coupling, (ii) ^{13}C magnetization is transferred to its ^{13}C neighbor(s) via $^1J_{CC}$ couplings, and (iii) ^{13}C magnetization is transferred back to ^1H via the $^1J_{CH}$ coupling. This is illustrated schematically in Figure 1A. The HCCH-COSY and HCCH-TOCSY experiments differ only in the mechanism used for ^{13}C–^{13}C magnetization transfer (i.e., step ii). In the case of the HCCH-COSY experiment, a 90° ^{13}C mixing pulse is used to transfer magnetization from a ^{13}C nucleus to its directly

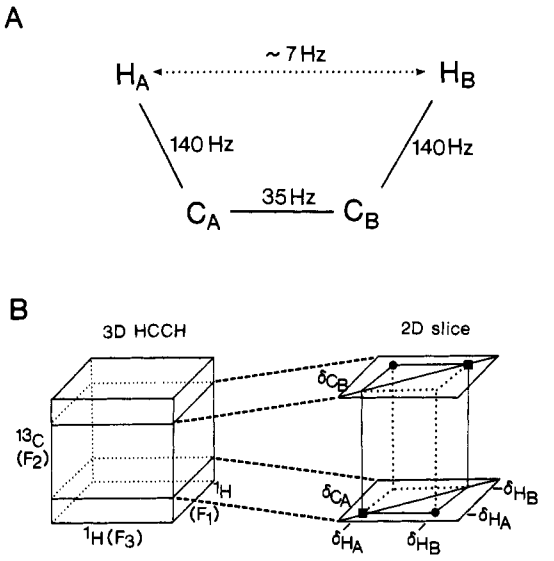

FIGURE 1: (A) Schematic representation of the ^1H–^{13}C–^{13}C–^1H spin system with typical coupling constants of $^1J_{CC}$, $^1J_{CH}$, and $^3J_{HH}$. (B) Schematic diagram of a 3D HCCH spectrum and its two slices at the ^{13}C (F_2) chemical shifts of the nuclei C_A and C_B, showing the diagonal and cross peaks expected for the simple spin system. The diagonal peaks are represented by squares and the cross peaks by circles.

bonded ^{13}C spins. On the other hand, the HCCH-TOCSY experiment relies on isotropic mixing of ^{13}C magnetization (Fesik et al., 1990) using an isotropic mixing scheme, DIPSI-3 (Shaka et al., 1988), that creates both direct and relayed magnetization transfer along the carbon chains. The power of these experiments for larger proteins stems (1) from the use of the well-resolved one-bond ^1H–^{13}C (~140 Hz) and ^{13}C–^{13}C (~35 Hz) J couplings to transfer magnetization, therefore overcoming the problems in conventional 2D COSY and HOHAHA techniques that rely on the poorly resolved ^1H–^1H (<12 Hz) J couplings and (2) from extension of the dimensionality from two to three, yielding a significant improvement in the spectral dispersion for the aliphatic region.

Each ^1H (F_1)–^1H (F_3) plane in the resulting 3D spectrum has an appearance similar to that of a 2D ^1H–^1H COSY or TOCSY experiment, while it is dispersed in the F_2 dimension by the ^{13}C chemical shift of the carbon nucleus directly attached to the ^1H at the diagonal position in the F_1–F_3-plane. This is schematically illustrated in Figure 1B. Here we consider the case where magnetization is transferred from proton A to proton B. In the plane corresponding to the ^{13}C chemical shift of the carbon A directly bonded to proton A, a cross peak is observed at

$$(F_1,F_2,F_3) = (\delta_{HA},\delta_{CA},\delta_{HB})$$

A symmetric cross peak can be observed at

$$(F_1,F_2,F_3) = (\delta_{HB},\delta_{CB},\delta_{HA})$$

in the plane corresponding to magnetization transfer from proton B to proton A. It should also be noted that diagonal peaks are only seen at the frequency of the proton where magnetization originates, i.e.,

$$(F_1,F_2,F_3) = (\delta_{HA},\delta_{CA},\delta_{HA})$$

and

$$(F_1,F_2,F_3) = (\delta_{HB},\delta_{CB},\delta_{HB})$$

On average, protons that resonate at high field are attached to high-field ^{13}C nuclei, and low-field ^1H resonances correlate with low-field ^{13}C resonances so that extensive folding in the ^{13}C (F_2) dimension can be used without the risk of introducing

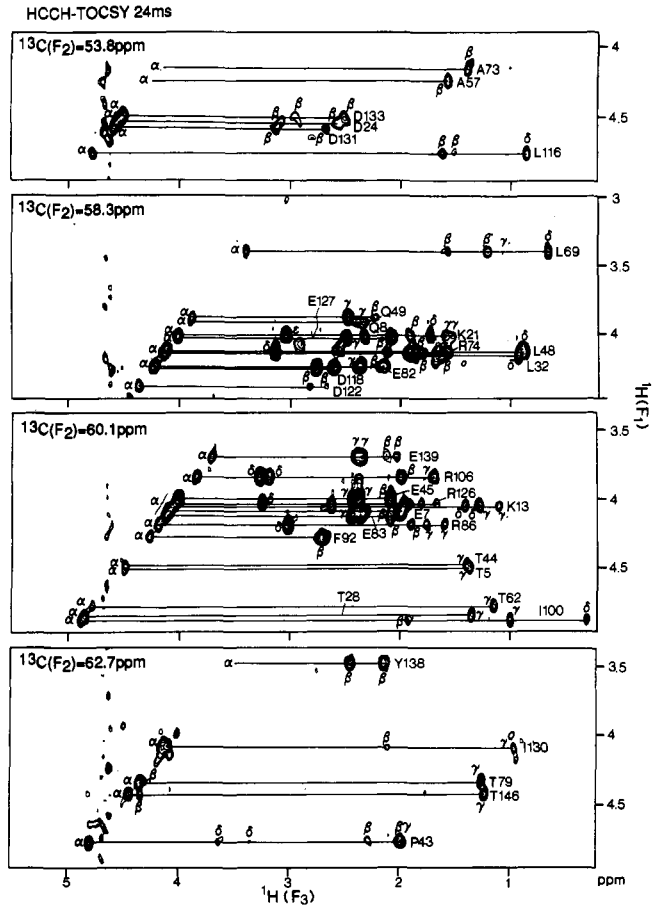

FIGURE 2: Selected slices at different ^{13}C (F_2) chemical shifts of the 24-ms HCCH-TOCSY spectrum of uniformly ^{15}N- and ^{13}C-labeled CaM, illustrating relayed connectivities originating from the CαH proton of several amino acid side-chain spin systems such as Ala, Asp, Leu, Glu, Gln, Lys, Arg, Thr, Ile, Phe, Tyr, and Pro.

ambiguities (Bax et al., 1991). In the present study, the spectral range of the ^{13}C (F_2) dimension was 23.8 ppm, and the carrier was positioned at 43.0 ppm. This affords reasonable digital resolution in the ^{13}C dimension with a limited number of data points (typically 32 complex).

The first step in the side-chain assignment process is to extend previous assignments of the CαH and $^{13}C\alpha$ resonances to the side-chain proton resonances. For this task, a particular region [F_1 (^1H) = 3.0–5.5 ppm, F_3 (^1H) = 0.0–5.5 ppm, F_2 (^{13}C) = 44–68 ppm] of the HCCH-COSY and 24-ms HCCH-TOCSY spectra is most important. On the basis of the CαH and $^{13}C\alpha$ assignments, it is relatively straightforward to identify the side-chain protons by combined use of the HCCH-COSY and HCCH-TOCSY 3D spectra in this region. Figure 2 illustrates several slices of the 24-ms HCCH-TOCSY 3D spectrum. The CβH and CγH resonances are distinguished by comparing the HCCH-COSY (data not shown) and HCCH-TOCSY spectra. Although the assignments are given for all the cross peaks in the figure, most important at this stage is to obtain the chemical shifts of the CβH protons for each amino acid residue. Ambiguity occurs when both CαH and $^{13}C\alpha$ chemical shifts of two residues are degenerate. In such cases, the ^{15}N HOHAHA-HMQC and ^{15}N ROESY-HMQC experiments frequently were used to resolve such problems. The ^{15}N HOHAHA-HMQC experiment often shows a correlation between HN and CβH protons via relayed magnetization transfer. The ^{15}N ROESY-HMQC experiment frequently shows a correlation from HN to CβH protons through the intraresidue ROE interaction. In the case of CaM, we found that the two experiments complement each other for this purpose.

Below we will focus on how the different amino acids can be identified with the HCCH method. As will be discussed, this identification relies in part on the characteristic Cα and Cβ chemical shifts of the various amino acids in random-coil peptides and in α-helical or β-sheet structures as reported by Spera and Bax (1991).

Glycine. The glycine spin systems in CaM could be identified by their unique connectivity pattern in the HCCH-COSY spectrum (supplementary material). The two CαH protons attached to the same $^{13}C\alpha$ carbon give a pattern symmetric about the diagonal in the slices taken perpendicular to the ^{13}C axis. The random-coil shift of the $^{13}C\alpha$ resonance is 45.1 ppm, while the 11 $^{13}C\alpha$ nuclei in CaM resonate in the range of 45.2–48.3 ppm. As will be discussed later, $^{13}C\alpha$ chemical shifts are clear markers for secondary structure. Residues in helical conformation typically resonate several parts per million downfield of their random-coil shift.

Alanine. In a conventional 2D COSY spectrum, every J correlation gives rise to two cross peaks appearing at mirror image positions with respect to the diagonal. In the 3D HCCH-COSY spectrum, however, the two cross peaks do not appear in the same ^{13}C slice because the carbons to which CαH and CβH$_3$ protons are attached resonate at different chemical shifts. The random-coil chemical shifts of $^{13}C\alpha$ and $^{13}C\beta$ resonances are 52.3 and 19.0 ppm, respectively. In the case of CaM, the $^{13}C\alpha$ chemical shifts of the 10 Ala residues range from 51.8 to 56.1 ppm. The carbon chemical shifts of both Cα methine and Cβ methyl groups help one to identify the unique Ala spin systems. Figure 3 illustrates the identification of the Ala spin system from the slice corresponding to the $^{13}C\alpha$ chemical shift (54.5 ppm).

Threonine. The spin system of threonine shows a linear connectivity pattern among the CαH, CβH, and CγH$_3$ protons in the HCCH-TOCSY spectrum. Figure 3 illustrates the identification of the complete spin systems of Thr-117 and Thr-146 in the 24-ms HCCH-TOCSY spectrum. The random-coil $^{13}C\alpha$ chemical shift of threonine is 62.1 ppm. The $^{13}C\alpha$ chemical shifts of 13 Thr residues in CaM range from 59.8 to 66.8 ppm. In the analysis of the conventional 2D COSY spectrum (data not shown), it was difficult to distinguish several of the Thr and Ala spin systems, in cases where no cross peak could be observed between the CαH and CβH protons of Thr. The difficulty in distinguishing Ala and Thr is completely removed in the present procedure using the HCCH-COSY and HCCH-TOCSY experiments. For example, although Thr-79 shows no obvious cross peak between the CαH and CβH (Figure 3), yielding a ^1H–^1H connectivity pattern similar to that of Ala, the $^{13}C\alpha$ shift (62.7 ppm) indicates that the spin system almost certainly corresponds to threonine. Further inspection of the slice corresponding to the $^{13}C\beta$ shift at 69.7 ppm (data now shown) indicates that the CαH and CβH chemical shifts are almost identical.

Serine. Serine belongs to the so-called AMX-type spin systems, and its $^{13}C\beta$ chemical shift (63.2 ppm in random coil) typically falls downfield from the $^{13}C\alpha$ chemical shift (58.2 ppm in random coil). The $^{13}C\alpha$ and $^{13}C\beta$ chemical shifts of the five Ser residues in CaM range from 55.9 to 61.7 ppm and from 63.1 to 66.4 ppm, respectively. Since the $^{13}C\beta$ chemical shifts of other AMX spin systems are at much higher field than those of Ser, the Ser spin systems are easily identified by their characteristic $^{13}C\alpha$, $^{13}C\beta$, and CβH chemical shifts.

Aspartic Acid and Asparagine. Asp and Asn conventionally are also designated as AMX spin systems. The random-coil

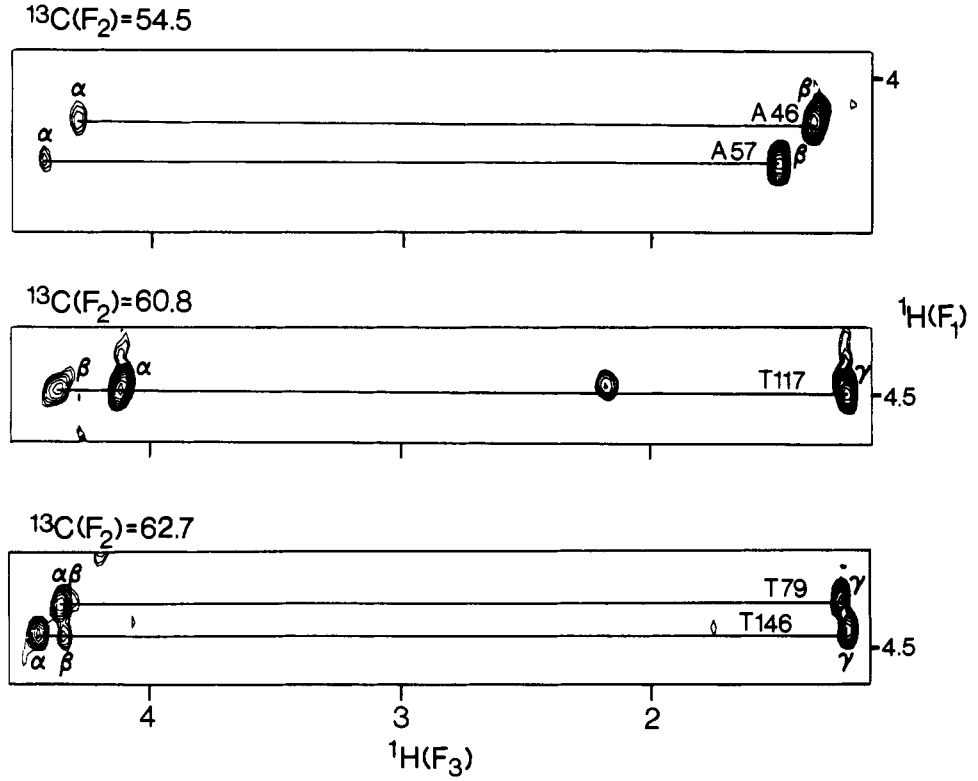

FIGURE 3: Selected slices at different ^{13}C (F_2) chemical shfits of the 24-ms HCCH-TOCSY spectrum of uniformly ^{15}N- and ^{13}C-labeled CaM, illustrating connectivities originating from the CαH of Ala and Thr residues. Note that the separation of $^{13}C\alpha$ chemical shifts between Ala and Thr is large, so that no ambiguity occurs for assigning Ala and Thr spin systems.

$^{13}C\alpha$ and $^{13}C\beta$ chemical shifts of Asp are 54.0 and 40.8 ppm, respectively, and those of Asn are 52.8 and 37.9 ppm. In the case of CaM, the $^{13}C\alpha$ chemical shifts of 16 Asp residues range from 52.3 to 57.6 ppm, and those of 7 Asn residues range from 51.2 to 56.0 ppm. Although computer similations of magnetization transfer for DIPSI-3 isotropic mixing (Clore et al., 1990a) indicate that a mixing time duration of 24 ms is longer than optimum for all the AMX-type spin systems, the 24-ms HCCH-TOCSY spectrum still offers an adequate signal-to-noise ratio, and a number of reasonably intense cross peaks originating from the CαH proton of Asp residues, including Asp-24, Asp-118, Asp-122, Asp-131, and Asp-133, can be observed (Figure 2).

In the ^{15}N–^1H shift correlation spectrum (data not shown), 11 pairs of cross peaks from the $CONH_2$ groups of Asn (43, 53, 60, 97, 111, and 137) and Gln (3, 8, 41, 49, and 135) are observed. The ^1H, ^{13}C, and ^{15}N chemical shifts of these $CONH_2$ groups were assigned on the basis of the NOE interaction between the amide protons and the terminal CH_2 group (CβH_2 for Asn and CγH_2 for Gln) observed in the 100-ms ^{15}N NOESY-HMQC spectra. Independent confirmation of these assignments was made by combined use of triple-resonance HNCO and HCACO 3D spectra (Kay et al., 1990a). Although both experiments are designed for obtaining backbone assignments (Ikura et al., 1990a), they also yield connectivities for the side-chain spin systems comprising CH_2CONH_2. The HNCO experiment yields the correlation from NH_2 protons to ^{13}CO via ^{15}N in the $CONH_2$ moiety. The HCACO experiment supplies the correlation from CH_2 protons to $^{13}CH_2$ carbon to ^{13}CO in the CH_2CO portion. Since the assignments of CβH_2 of Asn and CγH_2 of Gln are available from the HCCH experiment, all the ^1H, ^{13}C, and ^{15}N resonances in the $CONH_2$ groups can be assigned, provided the ^{13}CO chemical shifts are unique. Table IS (supplementary material) includes the assignment of the side-chain $CONH_2$ groups of the Asn residues.

Aromatic Amino Acids. The CαH–CβH_2 part of aromatic residues such as Phe, Tyr, His, and Trp also represents AMX spin systems. The random-coil $^{13}C\alpha$ and $^{13}C\beta$ chemical shifts of both Phe and Tyr are about 58.0 and 39.0 ppm, respectively. In the case of CaM, the $^{13}C\alpha$ chemical shifts of 10 aromatic residues (9 Phe and 1 Tyr) range from 55.9 to 63.7 ppm. The 24-ms HCCH-TOCSY spectrum (Figure 2) includes the correlations for Phe-92 at ^{13}C (F_2) = 60.1 ppm and for Tyr-138 at ^{13}C (F_2) = 62.7 ppm. The $^{13}C\beta$ shifts of Tyr and Phe are found in the region of 37.8–44.1 ppm. The single histidine residue in CaM (His-107) is easily identified because of its $^{13}C\beta$ shift (30.3 ppm), which is unique for AMX spin systems.

Partial ^1H aromatic assignments of CaM and its tryptic fragments have been reported previously (Ikura et al., 1984; Dalgarno et al., 1984). The present assignments agree with the earlier work. Since the aromatic carbons resonate at ~130 ppm, which is too far from the carrier placed at 43 ppm in the HCCH-COSY and HCCH-TOCSY experiments, no information on the ^{13}C shifts of aromatic groups is obtained from the HCCH experiments. The 2D ^1H–^{13}C HMQC spectrum showed that the majority of the nine Phe residues in CaM severely overlap except resonances of Tyr-138 and His-107, which are well-resolved. Therefore, we were not able to measure accurate values of aromatic ^{13}C shifts of most Phe residues. The assignments of the aromatic protons were largely based on the 3D ^{13}C NOESY-HMQC experiments where the NOE interactions could be observed between the aromatic protons and the neighboring aliphatic protons that have been assigned independently.

Valine. The spin system of Val yields a unique connectivity pattern among the aliphatic protons in the HCCH spectra. The random-coil $^{13}C\alpha$ chemical shift of Val is 62.3 ppm, and the $^{13}C\alpha$ chemical shifts of the seven Val residues in CaM range from 61.0 to 67.1 ppm. Figure 4 represents a slice of

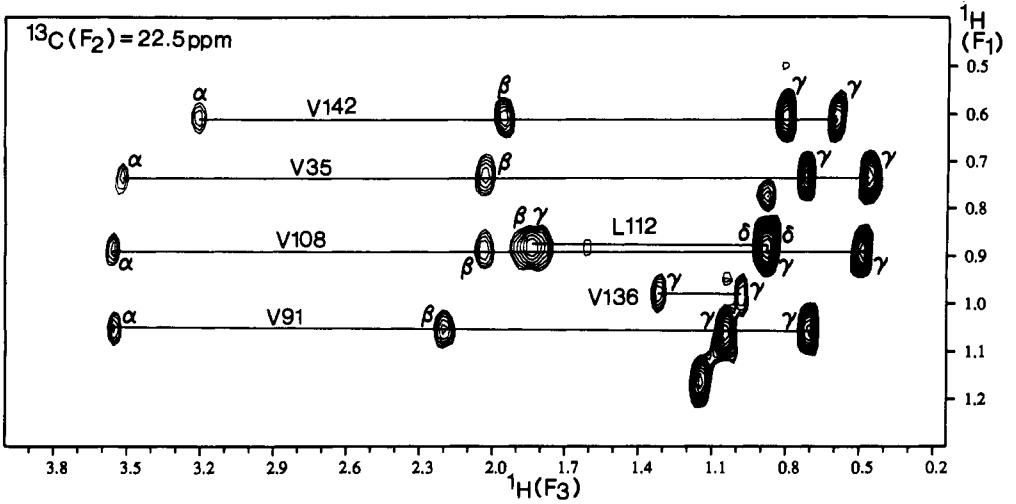

FIGURE 4: Slice of the 24-ms HCCH-TOCSY spectrum of uniformly ^{15}N- and ^{13}C-labeled CaM, illustrating connectivities involving Val spin systems. The correlations originate from the $C\gamma H_3$ protons of Val residues. The complete spin system is identified for five valines in this slice except for the $C\alpha H$ chemical shift of Val-136. In addition, this slice includes the correlations originating from the $C\delta H_3$ of Leu-112. The cross peak to the $C\alpha H$ proton (4.54 ppm) of Leu-112 is also observed but falls outside the window shown.

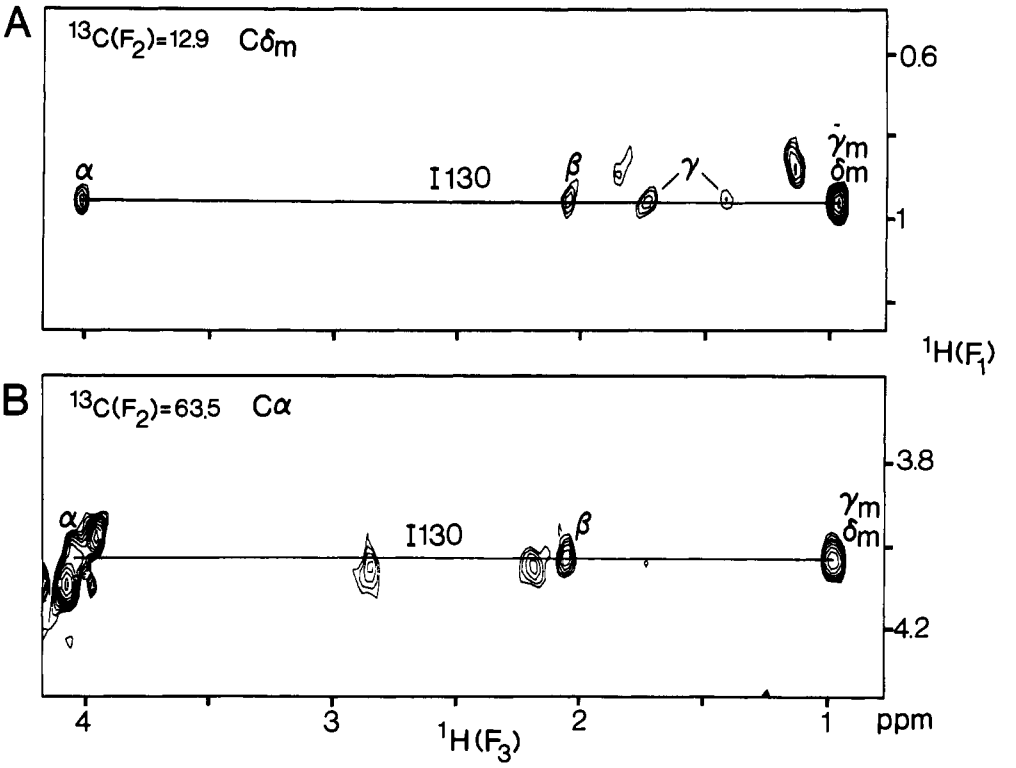

FIGURE 5: Selected slices at different ^{13}C (F_2) chemical shifts of the 24-ms HCCH-TOCSY spectrum of uniformly ^{15}N- and ^{13}C-labeled CaM illustrating the mirror image cross peaks originating from the $C\alpha H$ and $C\delta H_3$ protons of Ile-130. A similar connectivity pattern was observed in the slices corresponding to the $^{13}C\beta$ (38.7 ppm), $^{13}C\gamma$ (28.3 ppm), and $^{13}C_{\gamma m}$ (17.6 ppm) of Ile-130.

the 24-ms HCCH-TOCSY spectrum and shows connectivity patterns of five Val residues, each of which contains a $C\gamma$ methyl carbon resonating near F_2 = 22.5 ppm. The relayed connectivities from the $C\gamma H_3$ groups to the $C\beta H$, $C\alpha H$, and the second $C\gamma H_3$ yield the complete assignments of the valine spin systems.

Leucine. The spin system of Leu is somewhat more complicated than that of Val because of the insertion of a CH_2 group at the β position. However, the complete spin system of Leu is easily obtained by the HCCH method. The random-coil $^{13}C\alpha$ chemical shift of Leu is 55.1 ppm, and the $^{13}C\alpha$ chemical shifts of nine Leu residues in CaM range from 54.1 to 58.3 ppm. Figure 2 illustrates the identification of several Leu spin systems in the HCCH-TOCSY spectrum, including Leu-116 at ^{13}C (F_2) = 53.8 ppm and Leu-32, Leu-48, and Leu-69 at ^{13}C (F_2) = 58.3 ppm. Figure 4 includes the cross peaks for Leu-112 originating from $C\delta H_3$ to $C\gamma H$ and $C\beta H_2$. The cross peak between $C\delta H_3$ and $C\alpha H$ at 4.54 ppm is also observed in this slice of the 3D spectrum but falls outside the window used for the figure. It is noted that the two $^{13}C\delta$ chemical shifts of Leu are often substantially different, making them easy to identify in cases where the $C\delta H_3$ proton shifts are nearly identical.

Isoleucine. The Ile spin systems are most easily recognized by the "mirror image" analysis of the HCCH spectra. The random-coil $^{13}C\alpha$ chemical shift of Ile is 61.3 ppm, and the $^{13}C\alpha$ chemical shifts of eight Ile residues in CaM range from 60.1 to 64.9 ppm. Figure 5 illustrates the identification of the

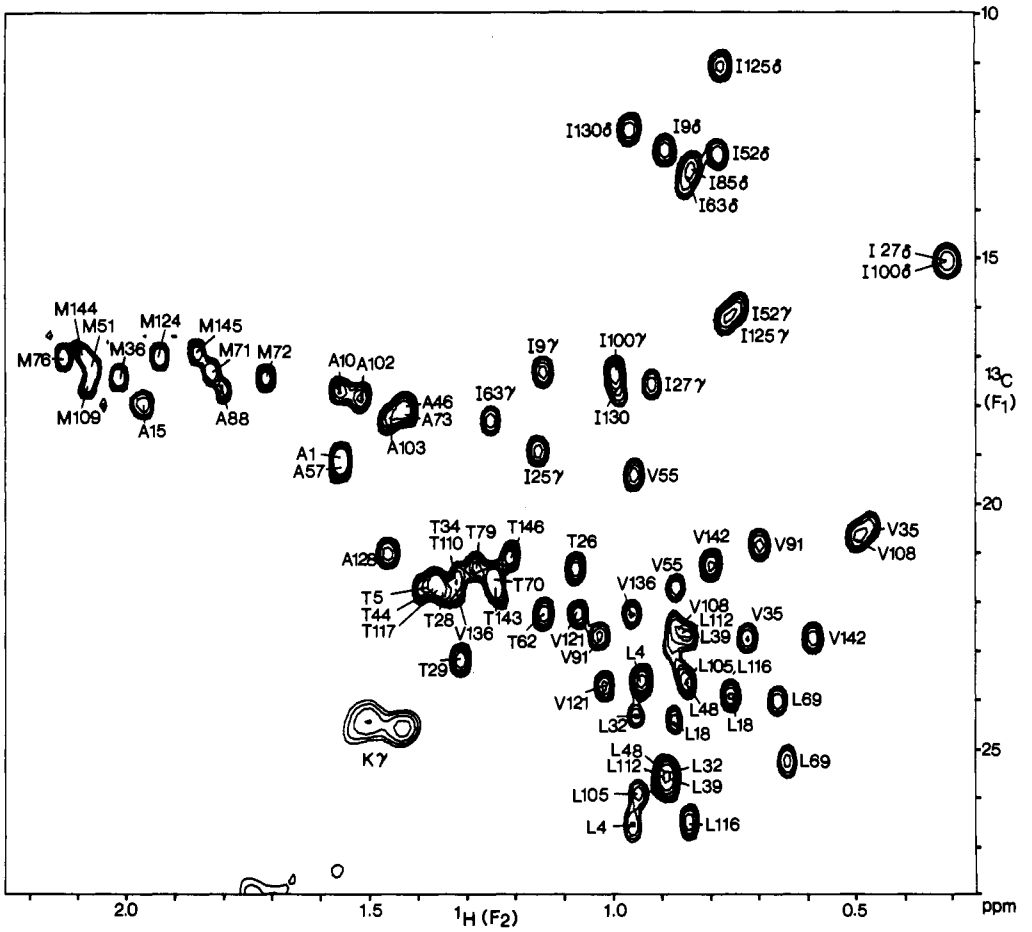

FIGURE 6: Methyl region of the ^{13}C–^{1}H HMQC spectrum of uniformly ^{15}N- and ^{13}C-labeled CaM. The assignments of the methyl groups of Met-71, -144, and -145 are tentative. The broad cross peak labeled by Kγ includes the $C\gamma H_2$ groups of Lys-21, Lys-30, Lys-75, Lys-77, Lys-94, Lys-115, and Lys-148. Accurate chemical shifts for these resonances were obtained from the 3D HCCH experiments (Table IS).

aliphatic resonances of Ile-130 using the mirror image pattern between the $^{13}C\alpha$ and $^{13}C_{\delta m}$. Although the $C\gamma H_2$ peaks are missing in the slice taken at the $^{13}C\alpha$ shift (Figure 5B), they can be identified in the slice originating from the $^{13}C_{\delta m}$ (Figure 5A). Further confirmation can be made by inspecting other slices corresponding to the $^{13}C\beta$, $^{13}C\gamma H_2$, and $^{13}C_{\gamma m}$ shifts (data not shown).

In this manner, all the amino acid residues containing methyl groups except methionines are assigned. Figure 6 shows the methyl region of the ^{1}H–^{13}C HMQC 2D spectrum, and the assignments of the methyl groups are summarized. The assignment of Met methyl groups will be discussed later.

Proline. CaM contains two Pro residues, Pro-43 and Pro-66. The random-coil $^{13}C\alpha$ chemical shift of Pro is 63.1 ppm, and the $^{13}C\alpha$ chemical shifts of Pro-43 and Pro-66 are 62.7 and 66.8 ppm, respectively. Figure 2 shows the spin system of Pro-43 at ^{13}C (F_2) = 62.7 ppm, including all the relayed cross peaks originating from the CαH. An ambiguity occurred for Pro-66, due to the identical chemical shifts between a pair of $C\beta H_2$ protons (2.23 and 1.94 ppm) and a pair of $C\gamma H_2$ protons (2.23 and 1.94 ppm). This has been resolved by examination of the 100-ms ^{13}C NOESY-HMQC spectrum, which exhibits clear intraresidue connectivities from nonequivalent CβH and CγH methylene protons at two slices corresponding to the $^{13}C\beta$ and $^{13}C\gamma$ shifts (data not shown). In the 24-ms HCCH-TOCSY, we could not observe the corresponding pattern, presumably due to weak intensities of these cross peaks.

The $^{13}C\gamma$ nuclei of Pro-43 and Pro-66 of CaM resonate at 27.5 and 28.5 ppm, respectively. In staphylococcal nuclease (Torchia et al., 1988a) and interleukin-1β (Clore et al., 1990a), the $^{13}C\gamma$ nuclei of *trans*-Pro residues resonate at 28.0 ± 2.0 ppm while $^{13}C\gamma$ of *cis*-Pro residues exhibits a relatively high-field shift (24.0 ppm for *cis*-Pro-117 in staphylococcal nuclease and 24.2 ppm for *cis*-Pro-91 in interleukin-1β). These data indicate that both Pro-43 and Pro-66 in CaM are in the trans conformation. Additional evidences for this conformation are CαH–CδH NOEs between Asn-42 and Pro-43 and between Phe-65 and Pro-66. No CαH–CαH NOE between these residues, which would be characteristic for *cis*-Pro, was observed for either proline. In the X-ray crystal structure (Babu et al., 1988), both prolines are also in the trans conformation.

Glutamic Acid and Glutamine. Glutamic acid and glutamine (Glx) are the most abundant residues in CaM (21 Glu and 5 Gln). The random-coil $^{13}C\alpha$ chemical shifts of the Glx residues are 56.4 and 56.1 ppm, respectively. The $^{13}C\alpha$ chemical shifts of 26 glutamates range from 53.2 to 60.4 ppm. The distribution of the $^{13}C\beta$ and $^{13}C\gamma$ chemical shifts is much narrower (see Figure 9) and causes an overlap problem even in the 3D spectra. The most useful assignment strategy, we find, is to start from the CαH and identify its coupled $C\beta H_2$ in the HCCH-COSY spectrum as well as the $C\gamma H_2$ in the HCCH-TOCSY spectrum. Figure 2 includes the spin systems of Glu 7, 45, 82, 83, 127, and 139 and Gln 8 and 49 residues. The accurate chemical shifts for the Cβ and Cγ carbons are often difficult to obtain, and the values listed in Table I allow an error of ±0.4 ppm. The $^{13}C\beta$ resonance of Glu-123 could not be identified.

The assignment of the $CONH_2$ moiety of glutamine residues was made as described in the section on asparagine. The

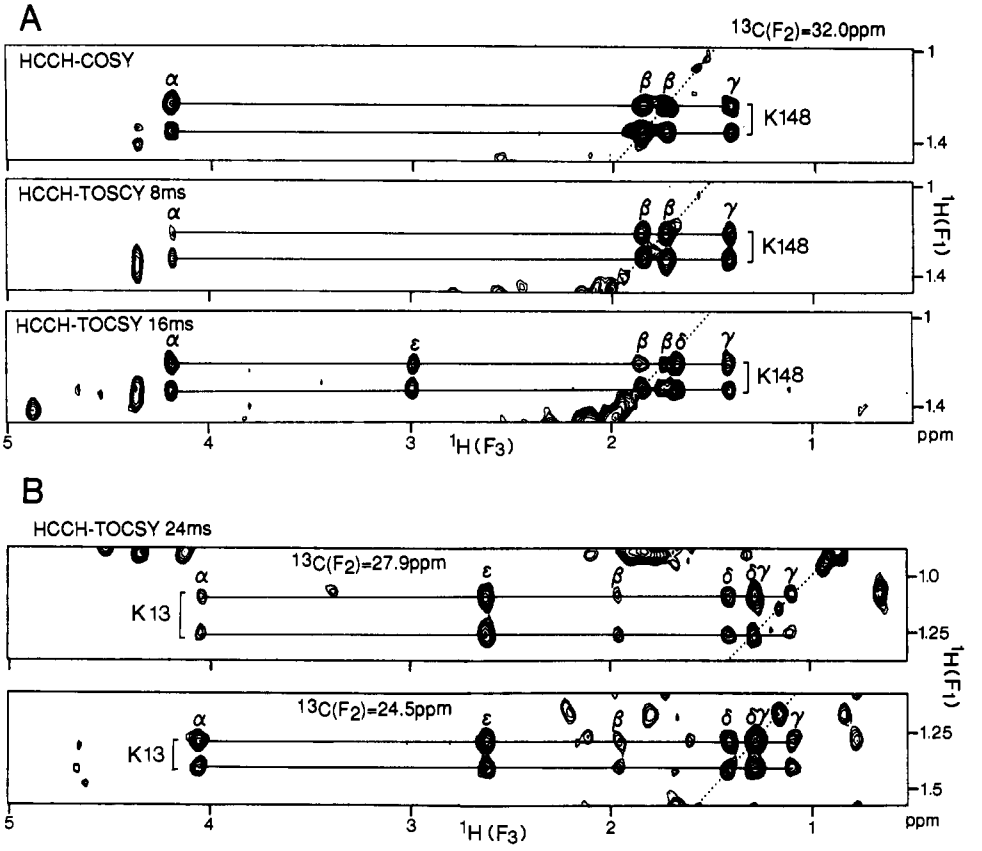

FIGURE 7: Selected slices at different ^{13}C (F_2) chemical shifts from several HCCH spectra of uniformly ^{15}N- and ^{13}C-labeled CaM illustrating relayed connectivities involving the spin systems of Lys-148 and Lys-13. (A) Slices are taken from the HCCH-COSY spectrum (top), the HCCH-TOCSY spectrum with an 8-ms mixing time (middle), and the HCCH-TOCSY spectrum with a 16-ms mixing time (bottom). All correlations originate from the $C\beta H_2$ of Lys-148. (B) Slices are taken from the HCCH-TOCSY spectrum with a 24-ms mixing time originating from the $C\gamma H_2$ protons (top) and from $C\delta H_2$ protons (bottom) of Lys-13.

chemical shifts are presented in Table IS (supplementary material). The assignments for Gln-8 and Gln-41 are tentative due to the absence of peaks in the 3D spectra and may be interchanged.

Methionine. The random-coil $^{13}C\alpha$ chemical shift of Met is 55.3 ppm, and the values of nine Met residues in CaM range from 55.9 to 59.4 ppm. Since the Met spin systems are similar to those of Glx, the complete assignment of the Met spin systems was complicated by the severe overlap with these Glx spin systems. The $^{13}C\beta$ of Met-36 and the $^{13}C\gamma$ resonances of Met-145 could not be identified.

The methyl protons and carbons of nine Met residues were assigned on the basis of the 3D ^{13}C-edited NOESY-HMQC spectrum. The assignment is based on the intraresidue NOEs between the methyl protons and the $C\alpha H$ and the $C\gamma H$ protons. All methionine residues except for Met-71 showed this type of NOE. In addition, interresidue NOEs were also used to confirm the assignment for Met-36, -51, -72, -76, -109, and -124. These NOEs are the following: Met-36 $C\epsilon H_3$ to Leu-32 $C\delta H_3$ and to Leu-39 $C\delta H_3$; Met-51 $C\epsilon H_3$ to Leu-48 $C\delta H_3$ and to Glu-47 $C\beta H_2$; Met-72 $C\epsilon H_3$ to Lys-75 $C\beta H_2$, $C\gamma H_2$, and $C\delta H_3$; Met-76 $C\epsilon H_3$ to Thr-79 $C\gamma H_3$; Met-109 $C\epsilon H_3$ to Val-108 $C\gamma H_3$ and to Leu-105 $C\delta H_3$; Met-124 $C\epsilon H_3$ to Ala-128 $C\beta H_3$. Table I includes the assignments of the Met methyl groups. The methyl groups of Met-144 and -145 are assigned on the basis of the intraresidue NOEs only and Met-71, by default, as the only remaining methyl resonance. The assignments for Met-144, -145, and -71 are therefore tentative at this stage. Evans et al. (1988) reported the assignment of the Met methyl protons in CaM based on studies of its proteolytic fragments and use of paramagnetic probes. Their assignment disagrees substantially with the present work. This discrepancy may reflect a possible difference in the local environment of Met side chains between intact CaM and its proteolytic fragments and/or the different nature of Ca^{2+} and lanthanide ions.

Lysine. With the conventional 2D method, it is frequently difficult to assign long aliphatic spin systems such as Lys and Arg, even for small proteins of less than 100 residues. For larger proteins the assignment of these residues becomes very difficult with conventional 2D methods because of (i) the increase in spectral overlap in the aliphatic region and (ii) the increase of ^1H line widths, which makes magnetization transfer through homonuclear ^1H–^1H couplings inefficient. In contrast, the HCCH-TOCSY spectra typically show correlations from each proton in the side chain to virtually all of the other resonances in the same side chain (Baldisseri et al., 1991). Consequently, complete spin systems can be traced easily starting from the different side-chain protons, thereby providing multiple checks on the assignments.

Figure 7A shows a comparison of the HCCH-COSY and HCCH-TOCSY spectra for Lys-148, which is the C-terminal residue. In the HCCH-COSY spectrum, correlations are observed from the $C\beta H_2$ protons only to the adjacent neighbors, $C\alpha H$ and $C\gamma H_2$. An identical pattern is observed with the HCCH-TOCSY experiment when an 8-ms mixing time is used (the middle panel in Figure 7A). The bottom panel shows the corresponding slice from the 16-ms HCCH-TOCSY spectrum where additional correlations from the $C\beta H_2$ to the $C\delta H_2$ and $C\epsilon H_2$ are observed.

Figure 7B shows two slices from the 24-ms HCCH-TOCSY spectrum taken at 27.9 and 24.5 ppm, corresponding to the

13Cγ and 13Cδ shifts of Lys-13. In this case, one of the nonequivalent $C\gamma H_2$ protons overlaps with one of the nonequivalent $C\delta H_2$ protons. This assignment is evident from the two spectra. Note that with homonuclear 2D ^1H NMR this assignment would be difficult to distinguish from a case with equivalent $C\gamma H_2$ protons at 1.28 ppm and equivalent $C\delta H_2$ protons at 1.40 ppm. In contrast with Lys-148, which has nonequivalent $C\beta H_2$ protons and equivalent $C\gamma H_2$ and $C\delta H_2$, Lys-13 has equivalent $C\beta H_2$ and nonequivalent $C\gamma H_2$ and $C\delta H_2$ resonances.

The random-coil $^{13}C\alpha$ chemical shift of Lys is 56.5 ppm. In the case of CaM, the $^{13}C\alpha$ chemical shifts of eight Lys residues range from 55.7 to 60.2 ppm.

Arginine. The analysis procedure as described for Lys above can also be used straightforwardly for Arg. The random-coil $^{13}C\alpha$ chemical shift of Arg is 56.1 ppm, and the $^{13}C\alpha$ chemical shifts of six Arg residues in CaM range from 58.9 to 60.1 ppm. Figure 2 includes the spin systems of Arg-86, Arg-106, and Arg-126.

In this manner, virtually complete side-chain spin systems can be identified for all 148 residues of CaM. Chemical shifts of the side-chain ^1H and ^{13}C resonances are summarized in Table IS (Supplementary material). These aliphatic ^{13}C side-chain assignments of CaM expand on the data base of ^{13}C chemical shifts in proteins that hitherto comprised mainly data reported for basic pancreatic trypsin inhibitor (Wagner & Bruhwiler, 1986), interleukin-1β (Clore et al., 1990a), and staphylococcal nuclease (Wang et al., 1990; Baldisseri et al., 1991). The present data are especially important for elucidating the correlation between ^{13}C chemical shifts and protein conformation, since CaM is the first protein rich in α-helix for which complete ^{13}C assignments are obtained. This complements the work performed on interleukin-1β, a protein rich in β-sheet.

Secondary Structure Analysis. The pattern of NOE connectivities identifies the nature of the polypeptide conformation (Wuthrich, 1986). Strong $d_{NN}(i,i+1)$ connectivities as well as $d_{\alpha N}(i,i+3)$ and $d_{\alpha\beta}(i,i+3)$ connectivities are indicative of an α-helical conformation. Both parallel and antiparallel β-sheet structures are associated with $d_{\alpha N}(i,i+1)$ and also with long-range $d_{\alpha N}(i,j)$ and $d_{NN}(i,j)$ connectivities between two polypeptide segments comprising the sheet. In this study, the 33-ms ^{15}N ROESY-HMQC and 50-ms ^{13}C NOESY-HMQC 3D spectra were used to identify the short-range and medium-range NOE connectivities, which are usually less than 4.0 Å. The 100-ms ^{15}N NOESY-HMQC and 100-ms ^{13}C NOESY-HMQC 3D spectra were used mainly to identify the medium- or long-range NOE connectivities that can correspond to interproton distances as long as 5 Å. In the case where two HN resonances are degenerate, such as those of Met-76 and Lys-77, the [^{15}N,^{15}N,^1H]HMQC-NOESY-HMQC 3D experiment (Ikura et al., 1990a; Frenkiel et al., 1990) was used to check the presence of the d_{NN} connectivity between the two degenerate HN resonances. In this manner, 10 pairs of $d_{NN}(i,i+1)$ connectivities not observable in the ^{15}N-edited NOESY-HMQC spectrum were established. These include Lys-30 and Glu-31, Met-36 and Arg-37, Gly-40 and Gln-41, Leu-48 and Gln-49, Met-76 and Lys-77, Val-91 and Phe-92, Leu-105 and Arg-106, Leu-112 and Gly-113, Val-121 and Asp-122, and Met-144 and Met-145. Figure 8 summarizes the short-range and medium-range NOEs as well as the information of slowly exchanging amide protons and the values of $^3J_{NH\alpha}$.

The size of $^3J_{NH\alpha}$ is related to the value of the φ torsional angle via a Karplus relationship (Karplus, 1963; Pardi et al., 1984). A small coupling constant (<5 Hz) is indicative of a value of φ between −80° and −40°, such as is commonly seen in α-helical structures. A large coupling constant (>8 Hz) suggests a φ value in the range −150° to −90°, consistent with an extended backbone conformation, as is the case in a β-sheet structure. Identification of slowly exchanging amide protons is used to help identify hydrogen-bonded NH groups within the protein. Typically, these are involved in well-defined secondary structure elements of both α-helix and β-sheet. The $^3J_{HN\alpha}$ values were obtained from the HMQC-*J* (method B) experiment (Kay & Bax, 1990) with uniformly ^{15}N-labeled CaM in H_2O (supplementary material). In total, 79 $^3J_{NH\alpha}$ coupling constants were obtained from resolved splittings. The smallest coupling constant that could be resolved was 4 Hz. For 53 amide protons, the *J* coupling was too small to be resolved. These unresolved $^3J_{HN\alpha}$ coupling constants are assumed to be smaller than 5 Hz. No values for the coupling constants were obtained for the remaining residues where cross peaks had a poor signal-to-noise ratio or exhibited resonance overlap.

The measurement of the exchange rates of the backbone amide protons was carried out by following the intensities of the ^1H–^{15}N correlation peaks in a series of double INEPT "Overbodenhausen" experiments (Marion et al., 1989) recorded at 25 °C after freeze-dried ^{15}N-labeled protein was dissolved in D_2O at pH 6.75. The first spectrum was recorded within 10 min, starting 5 min after the addition of D_2O to the protein. Amide protons with a hydrogen exchange rate k_{HX} smaller than $\sim 0.005\ s^{-1}$ can be detected in the first spectrum and are referred to as "slowly exchanging" amide protons. A total of 68 slowly exchanging amide protons were detected in 0.1 M KCl, pH 6.75, at 25 °C.

Figure 9 summarizes the ^{13}C chemical shifts observed for each type of amino acid in CaM. Comparison of this data base with that of interleukin-1β (Clore et al., 1990a) indicates that there is an obvious correlation between $^{13}C\alpha$ chemical shift and secondary structure. In the α-helical structures the $^{13}C\alpha$ nuclei resonate approximately 3 ppm downfield relative to their random-coil shifts, whereas in an extended structure such as β-sheet a small upfield shift is typically observed. Figure 8 includes a summary of the deviation of the $^{13}C\alpha$ chemical shifts from the random-coil values. It is clearly seen that there is a good agreement between the downfield shift of the $^{13}C\alpha$ resonances and α-helical conformation. The correlation between $^{13}C\alpha$ and $^{13}C\beta$ shifts and secondary structure has also been reported in solid-state NMR using synthetic poly(amino acids) [for a review, see Saito (1986)] and more recently has been demonstrated for four different proteins including CaM (Spera & Bax, 1991).

The eight Ile residues in CaM provide a clear example of the correlation between $^{13}C\alpha$ shift and secondary structure. Ile-27, Ile-63, and Ile-100 are involved in the short antiparallel β-sheet regions, and the $^{13}C\alpha$ chemical shift of those residues are 60.6, 60.1, and 60.4 ppm, respectively. Four Ile residues (Ile-9, Ile-52, Ile-85, and Ile-125) are located in α-helices, and the $^{13}C\alpha$ chemical shifts of these residues are 66.3, 64.9, 64.6, and 64.1 ppm, respectively. It is clearly seen that the averaged $^{13}C\alpha$ shift (65.0 ppm) in an α-helix is significantly downfield relative to that (60.4 ppm) in a β-sheet structure. This feature does not depend on the amino acid type. For example, the $^{13}C\alpha$ of Phe-99 in the antiparallel β-sheet also resonates substantially upfield (55.9 ppm) relative to the other eight Phe residues (60–65 ppm), all of which are in α-helices. A similar correlation between $^{13}C\beta$ shift and secondary structure is also observed but in the opposite way; the $^{13}C\beta$ resonances in the

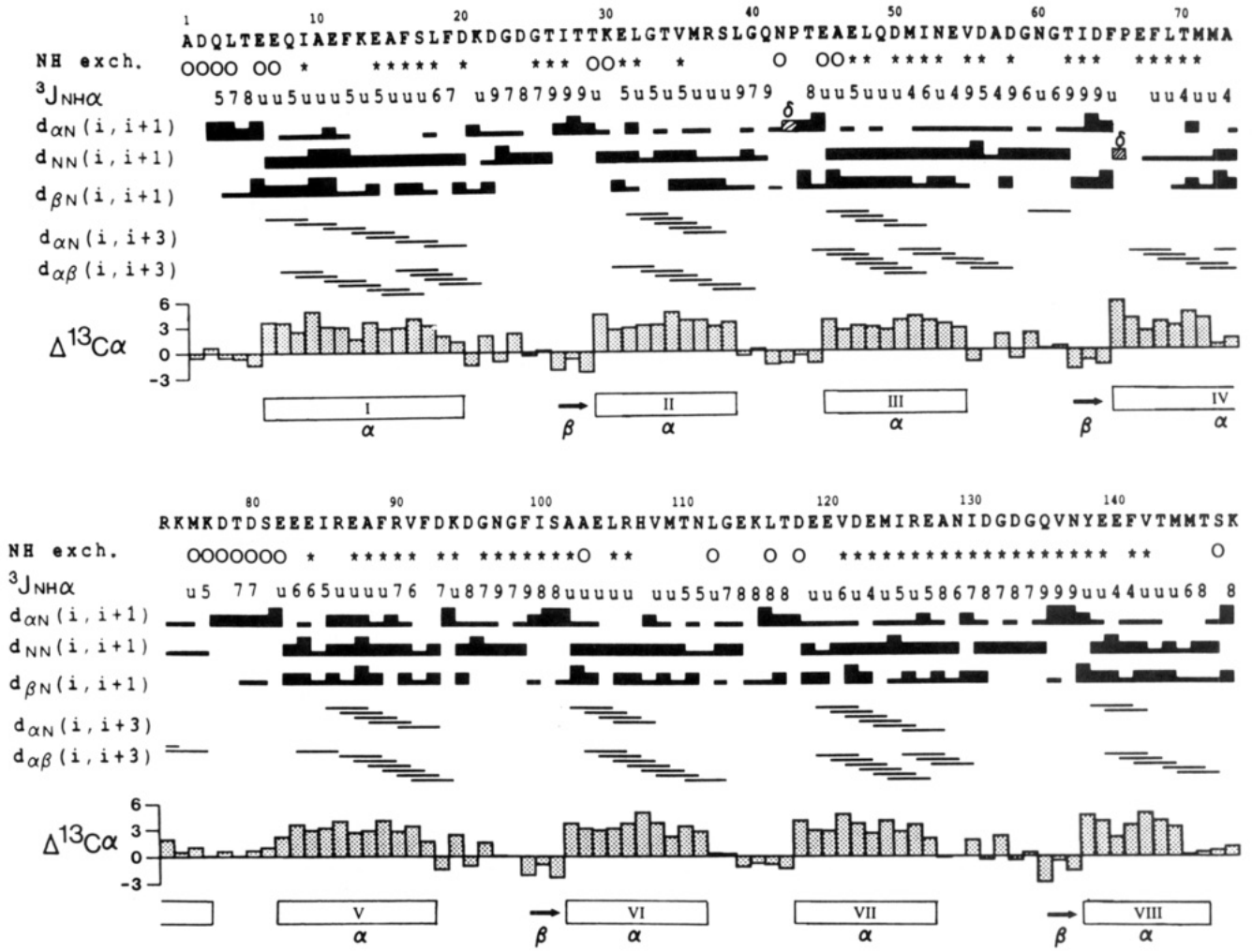

FIGURE 8: Amino acid sequence of *Drosophila* calmodulin and summary of the short- and medium-range NOEs involving HN, CαH, and CβH protons together with the slowly exchanging HN protons, the $^3J_{HN\alpha}$ coupling constants, and the secondary structure deduced from those data. In addition, the differences of the $^{13}C\alpha$ chemical shift of each amino acid residue and the random-coil shift (Spera & Bax, 1991) are plotted as a function of the residue number. The NOE intensities are indicated by the black bars and are classified according to the number of contour levels observed for each peak in the 3D NOESY-HMQC spectrum. A δ indicates that a NOE involves the CδH protons of a proline residue in place of an amide HN [i.e., $d_{\alpha\delta}(i,i+1)$]. Asterisks (*) indicate residues with amide HN resonances that are not fully exchanged 10 min after the protein is dissolved in D_2O at 25 °C and pH 6.75. Amides that exchange faster than 10 s^{-1} at pH 7.0, 35 °C, are marked by open circles. The $^3J_{HN\alpha}$ coupling constants (Hz) for each residue are indicated by numbers. Residues that exhibited an unresolved splitting in the HMQC-*J* spectrum (Kay & Bax, 1990) are indicated by "u". These are assigned the $^3J_{HN\alpha}$ coupling constant value of <5 Hz.

α-helical conformation appear upfield relative to the same residue in β-sheet structures (Spera & Bax, 1991).

α-Helical Structures. In addition to the strong or medium-size short-range $d_{NN}(i,i+1)$ connectivities and weak or absent $d_{\alpha N}(i,i+1)$ connectivities, the medium-range $d_{\alpha N}(i,i+3)$ and $d_{\alpha\beta}(i,i+3)$ backbone NOEs are used extensively for identification of α-helical structures. The medium-range $d_{\alpha N}(i,i+3)$ and $d_{\alpha\beta}(i,i+3)$ connectivities are often difficult to identify in conventional 2D NOESY spectra due to resonance overlap in the aliphatic region. The 3D ^{13}C NOESY-HMQC and ^{15}N NOESY-HMQC experiments, however, permit identification of many of the medium-range NOE connectivities, as shown in Figure 10. The slice taken from the ^{13}C NOESY-HMQC spectrum (Figure 10A) shows three $d_{\alpha\beta}(i,i+3)$ connectivities, between Leu-105 and Leu-108, between Glu-140 and Thr-143, and between Gln-49 and Ile-52. Figure 10A also includes Glu-82, which is in helix V, but the cross peak between its CαH and the Ile-85 CβH resonances is obscured because of the resonance overlap between the Glu-82 CβH_2 protons and the Ile-85 CβH proton. This $d_{\alpha\beta}(i,i+3)$ connectivity was, however, established by checking the mirror image cross peak on the slice at 37.5 ppm where the Ile-85 $^{13}C\beta$ carbon resonates. In addition, clear NOE cross peaks are observed between the Glu-82 CαH and the Ile-85 CγH3 and between the Glu-82 CαH and the Ile-85 CδH_3 as shown in Figure 10A. In the slice taken from the ^{15}N NOESY-HMQC spectrum (Figure 10B), two $d_{\alpha N}(i,i+3)$ connectivities are observed between Leu-48 HN and Glu-45 CαH protons and between Asp-50 HN and Glu-47 CαH protons.

Figure 8 illustrates the approximate locations of the eight helices elucidated by a qualitative interpretation of NMR data as described above. The eight helices are labeled I–VIII from the N-terminus. Table I compares the locations of the helices found in the present NMR work with those obtained from the X-ray diffraction study (Babu et al., 1988). With the exception of the end of helix IV and the start of helix V, the NMR and X-ray studies agree within an error of one residue. As pointed out by Clore and Gronenborn (1989), the accuracy of helix boundaries derived from the qualitative interpretation of NMR data is rather poor compared to the case of β-sheet. In addition, the definition of the exact start and end of helices in protein structures is somewhat indistinct.

However, the present NMR data clearly reveal the existence of the helix break in the region of Asp-78 to Ser-81 between

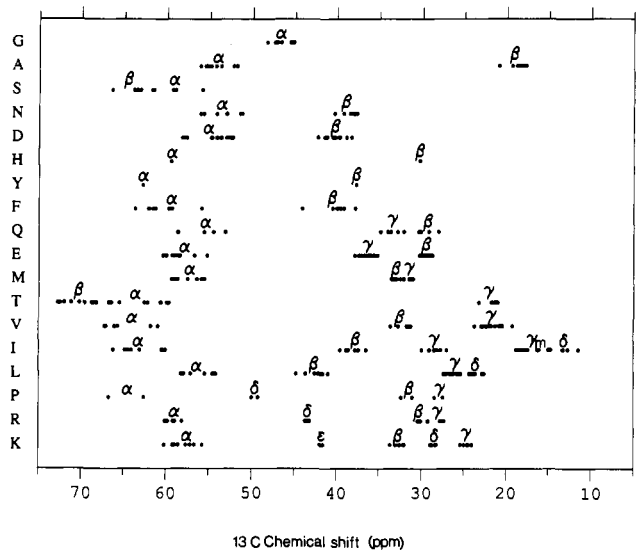

FIGURE 9: Summary of the ^{13}C chemical shift range observed for the different carbon atoms and different residue types in calmodulin.

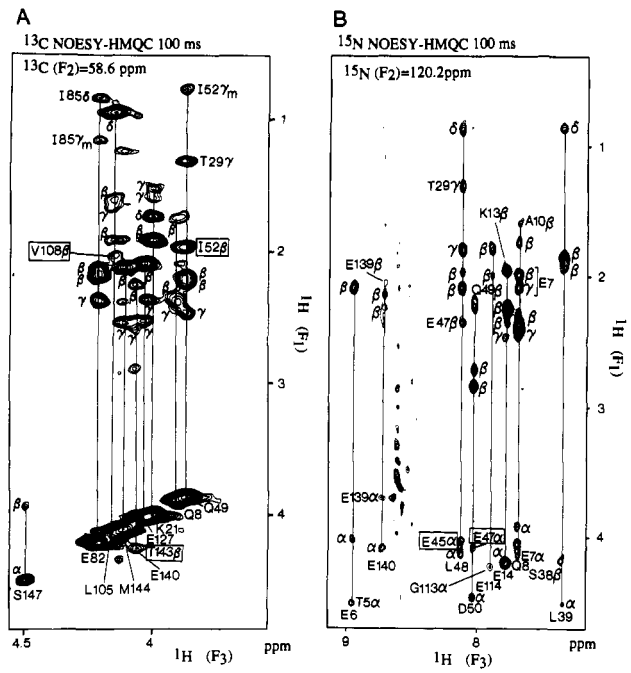

FIGURE 10: (A) Selected slice of the 100-ms ^{13}C NOESY-HMQC spectrum illustrating the $d_{\alpha\beta}(i,i+3)$ connectivities between Leu-105 CαH and Val-108 CβH, between Glu-140 CαH and Thr-143 CβH, and between Gln-49 CαH and Ile-52 CβH. The spectrum was obtained with uniformly ^{15}N- and ^{13}C-labeled CaM in D_2O. (B) Selected slice of the 100-ms ^{15}N NOESY-HMQC spectrum illustrating the $d_{\alpha N}(i,i+3)$ connectivities between Glu-45 CαH and Leu-48 HN and between Glu-47 CαH and Asp-50 HN. The spectrum was acquired with uniformly ^{15}N-labeled CaM in H_2O.

helices IV and V, which are part of the long central helix of the crystal structure (Babu et al., 1988; Kretsinger et al., 1986). Although in the crystalline state residues Thr-79 to Ser-81 show significant deviations in the ϕ and ψ dihedral angles from ideal α-helical geometry, the structure nevertheless shows a long straight helix from Phe-65 to Phe-92. The amide hydrogen exchange data as well as preliminary ^{15}N relaxation data (Barbato et al., unpublished results) suggest considerable mobility in the region from Asp-78 to Ser-81, which may account for the lack of medium-range NOEs for these residues. This is consistent with the small-angle X-ray scattering studies on CaM (Seaton et al., 1985; Heidorn & Trewhella, 1988; Matsushima et al., 1989). In addition, the temperature factors of this region in the X-ray crystal structure (Babu et al., 1988) are significantly larger (50–55 Å^2) than those of the globular lobes (20–30 Å^2).

Our recent study of amide hydrogen exchange kinetics in CaM (Spera et al., 1991) showed that the amide protons of Asp-2, Gln-3, Asn-42, Asp-78, Thr-79, Asp-80, and Ser-81 exchange rapidly with solvent ($k_{HX} > 50\ s^{-1}$ at pH 7.0, 35 °C). For these fast-exchanging amide protons, very few NOE cross peaks were observed in the ^{15}N NOESY-HMQC spectrum due to the magnetization exchange with the saturated H_2O resonance. Missing NOEs involving these fast-exchanging amide protons were, however, obtained by the 33 ms ^{15}N ROESY-HMQC experiment, which does not employ presaturation of the H_2O resonance. In the ROESY-HMQC spectrum, strong $d_{\alpha N}$ cross peaks were observed for Lys-77 and Asp-78; Asp-78 and Thr-79; Thr-79 and Asp-80; Asp-80 and Ser-81; Ser-81 and Glu-82. In this region, neither sequential $d_{NN}(i,i+1)$ connectivities nor medium-range $d_{\alpha N}(i,i+3)$ or $d_{\alpha\beta}(i,i+3)$ connectivities were observed.

β-Sheet Structures. The X-ray crystallographic studies (Babu et al., 1988; Kretsinger et al., 1986) and earlier NMR studies (Klevit et al., 1984; Ikura et al., 1985; Seeholzer & Wand, 1989) indicated that CaM contains two short antiparallel β-sheets. The present NMR study fully supports these observations. There are four short peptide segments consisting of three amino acid residues each (Thr-26 to Thr-28, Ile-63 to Phe-65, Phe-99 to Ser-101, and Gln-135 to Asn-137) that exhibit strong $d_{\alpha N}(i,i+1)$ connectivities and large $^3J_{NH\alpha}$ coupling constants (ca. 9 Hz), characteristic of β-sheet structures. In addition, all four pairs of three residues involved in the β-sheet conformation show a characteristic pattern of small upfield shifts of the $^{13}C\alpha$ resonances relative to their random-coil values (Figure 8).

Seeholzer and Wand (1989) reported the extensive 2D analysis of the interstrand NOEs in the antiparallel β-sheets of bovine brain CaM. Their results were fully confirmed in the present study. For example, the 100-ms ^{13}C NOESY-HMQC spectrum yielded $d_{\alpha\alpha}$ connectivities between Thr-26 and Asp-64 and between Phe-99 and Asn-137 (supplementary material). This characteristic NOE connectivity between a pair of Ca^{2+}-binding loops was recently observed even in a single Ca^{2+}-binding domain fragment of troponin C, which actually forms a symmetric homodimer in solution (Shaw et al., 1990; Kay et al., 1991). The other long-range NOEs between two Ca^{2+}-binding loops observed in the NOESY-HMQC spectra includes $d_{NN}(27,63)$, $d_{\alpha\alpha}(28,62)$, and $d_{NN}(100,136)$. The $d_{NN}(27,63)$ connectivity between the first and second Ca^{2+}-binding loops is analogous to the $d_{NN}(100,136)$ connectivity between the third and fourth Ca^{2+}-binding loops. The $d_{\alpha\alpha}(101,135)$ connectivity that corresponds to $d_{\alpha\alpha}(28,62)$ could not be established in this study, because of very similar CαH shifts of the two residues (4.90 ppm for Ser-101 and 4.88 ppm for Gln-135). This NOE interaction most likely could be observed by recording a 4D [^{13}C,^1H,^{13}C,^1H] HMQC-NOESY-HMQC spectrum (Clore et al., 1991; Zuiderweg et al., 1991), since the $^{13}C\alpha$ shifts of Ser-101 and Gln-135 (55.9 and 53.1 ppm, respectively) are different. All the observed NOEs for residues involved in the short β-sheets are in good agreement with the X-ray crystal structure (Babu et al., 1988; Kretsinger et al., 1986).

Ca^{2+}-Binding Loops. There are four Ca^{2+}-binding loops in CaM, which are well-characterized by the X-ray crystallographic studies (Babu et al., 1988; Kretsinger et al., 1986). In addition to the characteristic antiparallel β-sheet structure in the Ca^{2+}-binding loop regions, the hydrogen exchange experiments used in the present NMR study yield interesting

information on the nature of the Ca^{2+}-binding loops. As shown in Figure 8, the third and fourth Ca^{2+}-binding loops present in the C-terminal domain have a larger number of slow-exchange amide protons (a total of 18) than the first and second Ca^{2+}-binding loops of the N-terminal domain (a total of 6). The fourth Ca^{2+}-binding loop has the longest stretch of slow-exchanging amide protons starting from Val-121 to Glu-139. These results suggest that the Ca^{2+}-binding loops of the C-terminal domain are more resistant to cooperative unfolding (Englander et al., 1988) than the Ca^{2+}-binding loops in the N-terminal domain. The higher stability of the Ca^{2+}-binding loops in the C-terminal domain relative to their N-terminal counterparts may be correlated with the Ca^{2+}-binding affinity of each domain. Previous NMR (Ikura et al., 1983) and flow-dialysis studies (Minowa & Yagi, 1984) indicated that the third and fourth Ca^{2+}-binding loops in the C-terminal domain possess about 10-fold higher affinity for Ca^{2+} than the first and second Ca^{2+}-binding loops in the N-terminal domain.

Concluding Remarks. In this paper, we have described details of the side-chain ^1H, ^{13}C, and ^{15}N resonance assignments of CaM on the basis of the analysis of the HCCH-COSY and HCCH-TOCSY experiments as well as the NOESY-HMQC and triple-resonance experiments. The present results indicate not only that the ^{13}C chemical shift is useful for the separation of overlapping proton resonances in ^{13}C-separated 3D experiments but also that the ^{13}C chemical shift contains valuable information regarding protein conformation. In particular, $^{13}C\alpha$ and $^{13}C\beta$ chemical shifts appear to be reliable indicators for secondary structure. Although several previous studies (Clayden & Williams, 1982; Pardi et al., 1983; Wagner et al., 1983; Szilagyi & Jardetzky, 1989; Pastore & Saudek, 1990) suggest a correlation between protein conformation and proton chemical shifts of $C\alpha H$ and HN, in practice these proton chemical shifts are subject to substantial scatter caused by other structural features such as ring-current shifts from aromatic groups (Johnson & Bovey, 1958). However, since the distance between the center of an aromatic ring and a backbone $^{13}C\alpha$ carbon is at least several angstroms, the ring-current shift on the backbone carbon cannot exceed ~ 1 ppm. Moreover, the dispersion expressed in parts per million is much larger for ^{13}C than for ^1H resonances. Therefore, we believe that $^{13}C\alpha$ and $^{13}C\beta$ chemical shifts may become useful NMR parameters for secondary structure determination.

The secondary structure of CaM in solution has been shown to comprise four pairs of helix–loop–helix segments. The location of the two helices and the loop in each segment corresponds well to the EF-hand motif, which has been identified first for parvalbumin (Moews & Kretsinger, 1975). The most striking finding is that the central helix (Phe-65 to Phe-92) found in the crystal structure of CaM at 2.2–3.0-Å resolution (Babu et al., 1988; Kretsinger et al., 1986) has a flexible nonhelical region in solution for residues Asp-78 to Ser-81. Our preliminary analysis of long-range NOE data has not shown any NOE interactions between the N-terminal and C-terminal domains, indicating that the two domains probably do not interact directly on a time scale where NOE interaction can be observed. The flexible hinge between Asp-78 and Ser-81 may play an important role in allowing the two lobes of CaM to interact simultaneously with the target peptides and enzymes. Our recent NMR study on the complex between CaM and a 26-residue myosin light-chain kinase fragment (Ikura et al., 1991) indicates a significant change in the conformation of this region of the central helix upon complexation with the fragment as evidenced by changes in the NOE patterns, increased hydrogen exchange rates, and substantial chemical shift changes on backbone atoms. In the complex, the nonhelical region of the central helix involves residues Lys-75 through Ser-81. Further NOE analysis and NMR relaxation studies are currently in progress in order to characterize the structure and internal dynamics of this flexible hinge in more detail.

Acknowledgments

We thank Claude Klee for continuous help, encouragement, and stimulating discussions, Hans Vogel for fruitful discussion on the assignment of methiones, Kathy Beckingham and John Maune for providing us with the *Drosophila* calmodulin coding construct, Marius Clore, Paul Driscoll, Julie Forman-Kay, Angela Gronenborn, and Dennis Torchia for stimulating discussions, James Omichinski for expert help with the HPLC purification, Rolf Tschudin for skillfull assistance with the development of spectrometer hardware, and Ingrid Pufahl for valuable comments during the preparation of the manuscript. G.B. acknowledges L. Paolillo for continuous support.

Supplementary Material Available

Figure 1S showing the HCCH-COSY spectrum of ^{13}C- and ^{15}N-labeled CaM, depicting the spin systems of Gly-25, -98, and -40; Figure 2S showing the 2D HMQC-*J* spectrum of ^{15}N-labeled CaM; Table IS presenting the ^1H, ^{13}C, and ^{15}N resonance assignments of the side chains of CaM–$4Ca^{2+}$ at pH 6.3 and 36 °C (13 pages). Ordering information is given on any current masthead page.

References

Arrowsmith, C. H., Pachter, R., Altman, R. B., Iyer, S. B., & Jardetzky, O. (1990) *Biochemistry 29*, 6332–6341.

Babu, Y. S., Bugg, C. E., & Cook, W. J. (1988) *J. Mol. Biol. 204*, 191–204.

Baldisseri, D. M., Pelton, J. G., Sparks, S. W., & Torchia, D. A. (1991) *FEBS Lett.* (in press).

Bax, A., Griffey, R. H., & Hawkins, B. L. (1983) *J. Magn. Reson. 55*, 301–315.

Bax, A., Clore, G. M., Driscoll, P. C., Gronenborn, A. M., Ikura, M., & Kay, L. E. (1990a) *J. Magn. Reson. 87*, 620–627.

Bax, A., Clore, G. M., & Gronenborn, A. M. (1990b) *J. Magn. Reson. 88*, 425–431.

Bax, A., Ikura, M., Kay, L. E., & Zhu, G. (1991) *J. Magn. Reson. 91*, 174–178.

Bendall, M. R., Pegg, D. T., & Doddrell, D. M. (1983) *J. Magn. Reson. 52*, 81–117.

Clayden, N. G., & Williams, R. J. P. (1982) *J. Magn. Reson. 49*, 383–396.

Clore, G. M., & Gronenborn, A. M. (1989) *CRC Crit. Rev. Biochem. Mol. Biol. 24*, 479–564.

Clore, G. M., Bax, A., Driscoll, P. C., Wingfield, P. T., & Gronenborn, A. M. (1990a) *Biochemistry 29*, 8172–8184.

Clore, G. M., Bax, A., Wingfield, P. T., & Gronenborn, A. M. (1990b) *Biochemistry 29*, 5671–5676.

Clore, G. M., Kay, L. E., Bax, A., & Gronenborn, A. M. (1991) *Biochemistry 30*, 12–18.

Dalgarno, D. C., Klevit, R. E., Levine, B. A., Williams, R. J. P., Dobrowolski, Z., & Drabikowski, W. (1984) *Eur. J. Biochem. 138*, 281–289.

Driscoll, P. C., Clore, G. M., Marion, D., Wingfield, P. T., & Gronenborn, A. M. (1990) *Biochemistry 29*, 3542–3556.

Englander, J. J., Englander, S. W., Louie, G., Roder, H., Tran, T., & Wand, A. J. (1988) in *Structure and Expression: From Proteins to Ribosomes* (Sarma, R. H., & Sarma, M.

H., Eds.) Adenine Press, New York.
Evans, J. S., Levine, B. A., Williams, R. J. P., & Wormald, M. R. (1988) *Calmodulin*, pp 57–82, Elsevier, Amsterdam.
Fesik, S. W., & Zuiderweg, E. R. P. (1988) *J. Magn. Reson. 78*, 588–593.
Fesik, S. W., Eaton, H. L., Olejniczak, E. T., Zuiderweg, E. R. P., McIntosh, R. P., & Dahlquist, F. W. (1990) *J. Am. Chem. Soc. 112*, 886–888.
Frenkiel, T., Bauer, C., Carr, M. D., Birdsall, B., & Feeney, J. (1990) *J. Magn. Reson. 90*, 420–425.
Heidorn, D. B., & Trewhella, J. (1988) *Biochemistry 27*, 909–915.
Ikura, M., Hiraoki, T., Hikichi, K., Mikuni, R., Yazawa, M., Yagi, K. (1983) *Biochemistry 22*, 2568–2572.
Ikura, M., Hiraoki, T., Hikichi, K., Minowa, O., Yamazaki, H., Yazawa, M., Yagi, K. (1984) *Biochemistry 23*, 3124–3128.
Ikura, M., Minowa, O., & Hikichi, K. (1985) *Biochemistry 24*, 4264–4269.
Ikura, M., Bax, A., Clore, G. M., & Gronenborn, A. M. (1990a) *J. Am. Chem. Soc. 112*, 9020–9022.
Ikura, M., Kay, L. E., & Bax, A. (1990b) *Biochemistry 29*, 4659–4667.
Ikura, M., Kay, L. E., Tschudin, R., & Bax, A. (1990c) *J. Magn. Reson. 86*, 204–209.
Ikura, M., Marion, D., Kay, L. E., Shih, H., Krinks, M., Klee, C. B., & Bax, A. (1990d) *Biochem. Pharmacol. 40*, 153–160.
Ikura, M., Kay, L. E., Krinks, M., & Bax, A. (1991) *Biochemistry 30*, 5498–5504.
Johnson, C. E., & Bovey, F. A. (1958) *J. Chem. Phys. 29*, 1012–1014.
Karplus, M. (1963) *J. Am. Chem. Soc. 85*, 2870–2871.
Kay, L. E., & Bax, A. (1990) *J. Magn. Reson. 86*, 110–126.
Kay, L. E., Marion, D., & Bax, A. (1989) *J. Magn. Reson. 84*, 72–84.
Kay, L. E., Ikura, M., & Bax, A. (1990a) *J. Am. Chem. Soc. 112*, 888–889.
Kay, L. E., Ikura, M., Tschudin, R., & Bax, A. (1990d) *J. Magn. Reson. 89*, 496–514.
Kay, L. E., Forman-Kay, J. D., McCubbin, W. D., & Kay, C. M. (1991) *Biochemistry 30*, 4323–4333.
Klevit, R. E., Dalgarno, D. C., Levine, B. A., & Williams, R. J. P. (1984) *Eur. J. Biochem. 139*, 109–114.
Kretsinger, R. H., Rudnick, S. E., & Weissman, L. J. (1986) *J. Inorg. Biochem. 28*, 289–302.
Marion, D., Ikura, M., Tschudin, R., & Bax, A. (1989) *J. Magn. Reson. 85*, 393–399.
Matsushima, N., Izumi, Y., Matsuo, T., Yoshino, H., Ueki, T., & Miyake, Y. (1989) *J. Biochem. (Tokyo) 105*, 883–887.
McIntosh, L. P., Wand, A. J., Lowry, D. F., Redfield, A. F., & Dahlquist, F. W. (1990) *Biochemistry 29*, 6341–6362.
Messerle, B., Wider, G., Otting, G., Weber, C., & Wuthrich, K. (1989) *J. Magn. Reson. 85*, 608–613.
Minowa, O., & Yagi, K. (1984) *J. Biochem. (Tokyo) 96*, 1175–1182.
Moews, P. C., & Kretsinger, R. H. (1975) *J. Mol. Biol. 91*, 201–228.
Pardi, A., Wagner, G., & Wuthrich, K. (1983) *Eur. J. Biochem. 137*, 445–454.
Pardi, A., Billeter, M., & Wuthrich, K. (1984) *J. Mol. Biol. 180*, 741–751.
Pastore, A., & Saudek, V. (1990) *J. Magn. Reson. 90*, 165–176.
Saito, H. (1986) *Magn. Reson. Chem. 24*, 835–852.
Seaton, B. A., Head, J. F., Engelman, D. M., & Richards, F. M. (1985) *Biochemistry 24*, 6740–6743.
Seeholzer, S. H., & Wand, A. J. (1989) *Biochemistry 28*, 4011–4020.
Shaka, A. J., Barker, P. B., & Pines, A. (1988) *J. Magn. Reson. 77*, 274–293.
Shatzman, A. R., & Rosenberg, M. (1985) *Ann. N.Y. Acad. Sci. 478*, 233–248.
Shaw, G. S., Hodges, R. S., & Sykes, B. D. (1990) *Science 249*, 280–283.
Spera, S. & Bax, A. (1991) *J. Am. Chem. Soc. 113*, 5490–5492.
Spera, S., Ikura, M., & Bax, A. (1991) *J. Biomol. Nucl. Magn. Reson. 1*, 155–165.
Szilayi, L., & Jardetzky, O. (1989) *J. Magn. Reson. 83*, 441–449.
Torchia, D. A., Sparks, S. W., & Bax, A. (1988) *J. Am. Chem. Soc. 110*, 2320–2321.
Torchia, D. A., Sparks, S. W., & Bax, A. (1989) *Biochemistry 28*, 5509–5524.
Wagner, G., & Bruhwiler, D. (1986) *Biochemistry 25*, 5839–5834.
Wagner, G., Pardi, A., & Wuthrich, K. (1983) *J. Am. Chem. Soc. 105*, 5948–5949.
Wang, J., Hinck, A. P., Loh, S. N., & Markley, J. L. (1990) *Biochemistry 29*, 102–113.
Wuthrich, K. (1986) *NMR of Proteins and Nucleic Acids*, Wiley, New York.
Zuiderweg, E. R. P., & Fesik, S. W. (1989) *Biochemistry 28*, 2387–2391.
Zuiderweg, E. R. P., Petros, A. M., Fesik, S. W., & Olejniczak, E. T. (1991) *J. Am. Chem. Soc. 113*, 370–372.